Complex-Valued Neural Networks for Privacy Protection

Liyao Xiang ¹ Haotian Ma ² Hao Zhang ¹ Yifan Zhang ¹ Quanshi Zhang ¹³

Abstract

This paper proposes a generic method to revise traditional neural networks for privacy protection. Our method is designed to prevent inversion attacks, i.e. avoiding recovering private information from intermediate-layer features of a neural network. Our method transforms real-valued features of an intermediate layer into complex-valued features, in which private information is hidden in a random phase of the transformed features. To prevent the adversary from recovering the phase, we adopt an adversarial-learning algorithm to generate the complex-valued feature. More crucially, the transformed feature can be directly processed by the deep neural network, but without knowing the true phase, people cannot recover either the input information or the prediction result. Preliminary experiments with various neural networks (including the LeNet, the VGG, and residual networks) on different datasets have shown that our method can successfully defend feature inversion attacks while preserving learning accuracy.

1. Introduction

Deep neural networks (DNNs) have shown superb capabilities to process different types of local devices such as mobile phones, medical equipment, Internet of Things (IoT) devices have become the data entry points in recent years. Although on-device machine learning has exhibited various advantages, it usually burdens the thin devices with overwhelming computational overhead. Yet, offloading raw data to the cloud would put the individual privacy at risk. Hence a trade-off solution is to offload intermediate feature representations, rather than the raw data, to the cloud for further processing.

However, as shown in (Dosovitskiy & Brox, 2016),

intermediate-layer features are subject to inversion attacks, *i.e.* recovering the input data from features of intermediate layers. It means that an adversary can launch attacks to recover any sensitive information in the input from the offloaded features on the cloud.

Therefore, in this paper, we propose a novel method to revise a traditional neural network into a privacy-preserving complex-valued neural network. Note that the network is termed a complex-valued neural network, because features in intermediate layers are complex-valued for privacy protection, rather than that network parameters are complex-valued.

We release intermediate-layer complex-valued features to the cloud without significant privacy leaks. As shown in Fig. 1, the entire network can be divided into the following three modules.

• The encryption module is embedded inside a local device of a human user. The encryption module extracts features from the input, encrypts the features, and sends the encrypted features to the cloud.

For conciseness, we slightly abuse terms such as *encryption* and *decryption* without confusing them with their counterparts in cryptographic contexts.

- The processing module is located on the public cloud.
 This module receives and processes the encrypted feature without knowing the secret key and returns the processed feature back to the human user.
- The decryption module on the local device of a user receives and decrypts the processed features and generates the final result.

We face two significant challenges in the above inference process. First, the feature f in the intermediate layers contains considerable sensitive information about the input I, which can be recovered by an adversary who trains a decoder neural network g such that $\hat{I} = g(f)$. Our objective is to design f such that the adversary cannot well recover I from f.

Second, ensuring that the encrypted feature can be processed by the neural network without sacrificing the utility

¹John Hopcroft Center, Shanghai Jiao Tong University, China ²Southern University of Science and Technology, China ³MoE Key Lab of Artificial Intelligence, AI Institute, Shanghai Jiao Tong University, China. Correspondence to: Quanshi Zhang <zqs1022@sjtu.edu.cn>.

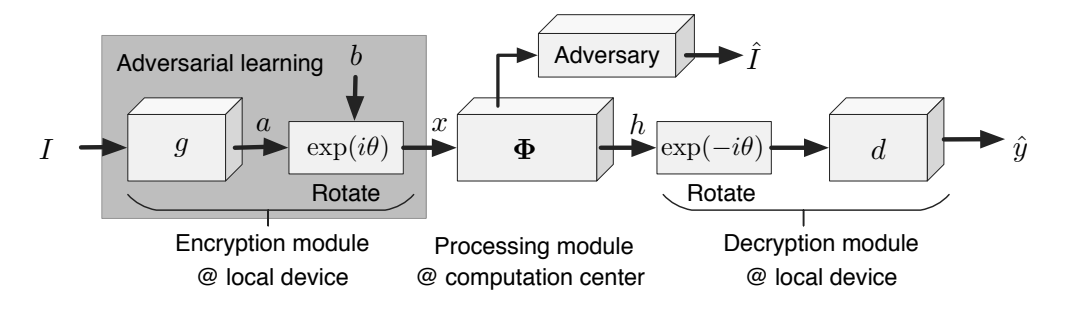


Figure 1. Structure of the complex-valued neural network.

too much presents another great challenge. Different network structures are designed to handle different types of data — convolutional neural networks (CNNs) are designed for images, and recurrent neural networks (RNNs) mainly deal with sequential data. Piecewise linear feature representations in neural networks are widely believed not suitable to handle strict high-order logic. Hence our second objective is to let the encrypted feature be processable by the neural network.

We propose to hide the private information of the input in a random phase of a complex-valued feature. Given a neural network for a certain task, we develop a simple-yeteffective method to adapt the neural network for processing the complex-valued features. Note that the same training data is required to train such a neural network as the original neural network, without a need for any additional human annotations.

More importantly, to prevent the true phase corresponding to the feature from being re-identified, we use adversarial learning to synthesize complex-valued features, so that the real feature can be hidden better. Without knowing the phase, any adversary cannot obtain either the private input or the final output given the intermediate-layer feature.

Contributions of this study can be summarized as follows. We propose a novel method which transforms a traditional neural network into a complex-valued one, such that the adversary cannot recover input information from the intermediate-layer features. Our complex-valued neural network is verified by experiments on various datasets and network structures to be able to successfully defend feature inversion attacks with a very limited decrease of the task accuracy.

2. Related Work

Complex-valued neural networks. Using complex-valued features or complex-valued parameters in neural networks has always been an interesting topic. From the computa-

tional perspective, complex-valued neural networks have a competitive performance with their real-valued counterparts (Trabelsi et al., 2018). By augmenting recurrent neural networks with associative memory based on complex-valued vectors, (Danihelka et al., 2016) achieved faster learning on memorization tasks. Complex-valued features can contain information in both the phase and the magnitude. An example is that Reichert *et al.* used the phase to indicate properties of spike timing in cortical information processing (Reichert & Serre, 2013). In our research, the phase contains the user's private information without which the original feature of the input cannot be exactly identified.

Inversion attacks. The intermediate-layer features released to the public have been shown to be vulnerable to inversion attacks (Dosovitskiy & Brox, 2016). To invert intermediate-layer features, a typical method (Dosovitskiy & Brox, 2016) is to train a decoder with up-convolutional layers to reconstruct the input. Given parameters of a pre-trained model, gradient-based visualization (Zeiler & Fergus, 2014; Mahendran & Vedaldi, 2015; Simonyan et al., 2013) can be used for reconstruction. Whereas, without knowing model parameters, the model-agnostic decoder network is usually used to recover private inputs.

Privacy-preserving deep learning. Various privacypreserving mechanisms have been proposed using different definitions of privacy: (Osia et al., 2017) applied the Siamese architecture to separate the primary and private information so that the primary information was preserved in the feature. PrivyNet (Li et al., 2017) was proposed to decide the local neural network structure under the privacy constraint based on the peak signal-to-noise ratio or the pixel-wise Euclidean distance. Data nullification and random noise addition were introduced by (Wang et al., 2018) to protect private information in the features, which guaranteed differential privacy. (Shokri & Shmatikov, 2015) and (Abadi et al., 2016) proposed privacy mechanisms based on the differentially-private stochastic gradient descent (Song et al., 2013) to prevent the adversary with arbitrary side information from telling private inputs.

Cryptographic tools have been used to learn from the sensitive data. Zhang *et al.* (Zhang et al., 2016) adopted homomorphic encryption, in particular, BGV encryption, to encrypt the private data and perform the high-order backpropagation on the encrypted data; (Mohassel & Zhang, 2017) distributed the private data among two non-colluding servers who performed the secure two-party computation to train models on the joint data.

The privacy definition suggested by our work is similar to k-anonymity in the sense that the adversary could reconstruct at least k different inputs from a transformed feature so that the adversary would be confused in identifying the correct input from reconstruction results.

3. Algorithm

The structure of our privacy-preserving neural network is shown by Fig. 1, which consists of an encryption module, a processing module, and a decryption module. The three modules are jointly trained as a single neural network. During the inference, the encryption and decryption modules are placed on local devices, while the processing module is located on the computational cloud for public use.

Let $I \in \mathbf{I}$ denote an input in the dataset and g be the encryption module at the local device. The feature of I is computed locally as

$$a = g(I), \tag{1}$$

but we do not directly release a. Instead, we introduce a fooling counterpart b, which we will elaborate later to construct the complex-valued feature

$$x = \exp(i\theta) [a + bi], \tag{2}$$

where the angle θ is randomly chosen and only known by the local device. The fooling counterpart b is selected such that it does not contain any private information of a, and it is sufficient to cause confusion. The encrypted feature is then sent to the processing module Φ for further processing. The processing module sends the processed feature $h = \Phi(x)$ back to the local device, which is also a complex value. Upon receiving h, the decryption module in the local device decrypts h as follows.

$$\hat{y} = d(\Re[\exp(-i\theta) \cdot h]). \tag{3}$$

d can be the last few layers of the neural network or just a softmax layer, depending on the amount of information to be processed locally. $\Re(\cdot)$ denotes the operation of picking real parts of complex values.

Overall, the entire neural network $[g, \Phi, d]$ should be trained over the original training dataset without any additional supervision. Once trained, all parameters of the three modules

may be publicly known. At the inference, the local device secretly selects a fooling counterpart b and the rotation angle θ to encrypt its feature. In later sections, we will focus on the encryption method, which ensures that the encrypted complex-valued feature x can be properly handled by Φ and d.

3.1. Processing Module

The key challenge of designing the processing module Φ is that the complex-valued feature should be adapted to the neural network operations. The objective is that if we rotate the complex-valued feature a+bi by an angle θ , all intermediate-layer features are rotated by the same angle. We represent the processing module as cascaded functions of multiple layers $\Phi(x) = \Phi_n(\Phi_{n-1}(\cdots \Phi_1(x)))$, where $\Phi_j(\cdot)$ denotes the function of the j-th layer. Let $f_j = \Phi_j(f_{j-1})$ represent the output feature of the j-th layer. Thus, the processing module should hold the following property:

$$\Phi(f^{(\theta)}) = e^{i\theta} \Phi(f)$$
s.t. $f^{(\theta)} \stackrel{def}{=} e^{i\theta} f, \forall \theta \in [0, 2\pi).$ (4)

In other words, the function of each intermediate layer in the processing module should satisfy

$$\Phi_{j}(f_{j-1}^{(\theta)}) = e^{i\theta} \Phi_{j}(f_{j-1})$$
s.t. $f_{j-1}^{(\theta)} \stackrel{def}{=} e^{i\theta} f_{j-1}, \ \forall j \in [2, \dots, n], \ \forall \theta \in [0, 2\pi).$

$$(5)$$

to recursively prove Eqn. (4).

Let us consider six most common types of network layers to construct the processing module, *i.e.* the conv-layer, the ReLU layer, the batch-normalization layer, the average/max pooling layer, the dropout layer, and the skip-connection operation. For the conv-layer, we remove the bias term and obtain $\operatorname{Conv}(f) = w \otimes f$ to satisfy Eqn. (5).

We replace the ReLU with the following non-linear layer:

$$\delta(f_{ijk}) = \frac{\|f_{ijk}\|}{\max\{\|f_{ijk}\|, c\}} \cdot f_{ijk} \tag{6}$$

where f_{ijk} denotes the neural unit at the location (i, j) in the k-th channel of the feature map, and c is a hyper-parameter.

The batch-normalization operation is replaced by

$$norm(f_{ijk}^{l}) = \frac{f_{ijk}^{l}}{\sqrt{\mathbb{E}_{ijl}[\|f_{ijk}^{l}\|^{2}]}},$$
 (7)

where f^l denotes the complex-valued tensor for the l-th sample in the batch.

For max-pooling layers, we modify the rule such that the neural activation unit with the maximum norm in the region is selected. The modified max-pooling layer does not change the phase of its input. For the dropout layer, we apply the dropout operation at the unit of each individual complex value with both the real part and the imaginary part. Skip connections can be formulated as $f + \Phi(f)$, where the inner module $\Phi(f)$ also satisfies Eqn. (4).

All above six operations satisfy Eqn. (4). Please see supplementary materials for the proof.

3.2. Encryption Module

The objective of the encryption module is to hide the real feature a of the input I in a certain phase θ^* of the encrypted complex-valued feature $x = \exp(i\theta^*) \left[a + bi \right]$. Let $a' = \Re[x \exp(-i\theta')] = \Re[(a+bi) \exp(i\theta^* - i\theta')] = \Re[(a+bi) \exp(i\Delta\theta)]$ denote a fake feature that is decrypted using a random angle $\theta' \neq \theta^*$, where $\Delta\theta = \theta^* - \theta'$. A successful encryption requires (i) the fake feature a' contains little information of the real feature a; (ii) the fake feature a' and the real one a follow the same distribution so that it is difficult to distinguish the real feature from fake ones.

Therefore, we can formulate the encryption problem using the following adversarial loss:

$$\min_{g,\{b_I|b_I\neq a,I\in\mathbf{I}\}} \max_{D} L(g,\{b_I\},D)$$
s.t.
$$L(g,\{b_I\},D) = \sum_{I\in\mathbf{I}} \left\{ D(a) - \mathbb{E}_{a'\neq a} \left[D(a') \right] \right\}$$

$$= \sum_{I\in\mathbf{I}} \left\{ D[g(I)] - \mathbb{E}_{\Delta\theta\neq0} \left[D\left[\Re[(g(I) + b_I i) \exp(i\Delta\theta)] \right] \right] \right\}.$$
(8)

In the adversarial learning module, a discriminator network D is learned to classify the real feature a from the fake feature a'. We follow the technical setting of the W-GAN (Arjovsky et al., 2017) to implement the adversarial learning to generate features. The encryption module g is trained along with the imaginary part of the feature b_I to fool the discriminator D, while D is trained to distinguish a and a'.

Thus, the overall loss for learning is given as follows:

Loss =
$$L(g, \{b_I\}, D) + L^{\text{task}}(\hat{y}, y^*)$$
 (9)

where $L^{\text{task}}(\hat{y}, y^*)$ represents the task loss over the targeted output y^* .

Note that to simplify the implementation, we compute $b_I = g(I')$ as the feature of a randomly chosen sample $I' \neq I$, to fool the discriminator. In this way, the estimation of b_I in Eqn. (8) is absorbed in the optimization of the encryption module g. Since the expectation in Eqn. (8) is taken over all possible $\Delta\theta \neq 0$, in practice, we sample k-1 nonzero values of $\Delta\theta$, and iterate through these k-1 values

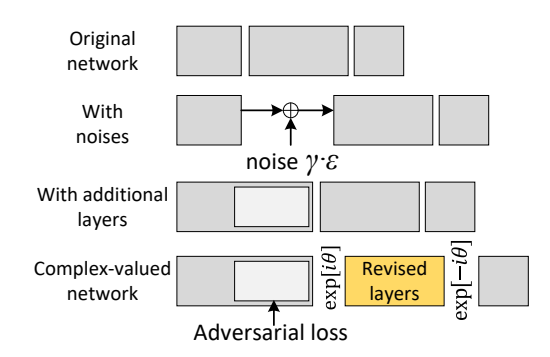


Figure 2. Overview of baseline network structures.

as negatives in the adversarial learning. The adversarial-learning module ensures that at least k-1 fake features are generated resembling the real one, *i.e.* when an adversary tries to recover a from x by reverting an arbitrary angle θ' , it would recover at least k-1 other features along with a.

Understanding the feature encryption from the perspective of inversion-attack strategies: The adversarial loss in Eqn. (8) can explain the effectiveness of the complex-valued feature in privacy protection concerning two inversion attack strategies.

Strategy 1: The adversary tries to find out the most likely rotated angle $\hat{\theta}$ to revert the feature x to obtain a, and inverting a by a decoder network dec such that $\hat{I} = \text{dec}(\Re[x\exp(-i\hat{\theta})])$. An example is to build a discriminator D' such that $\hat{\theta} = \max_{\theta} D'(\Re[x\exp(-i\theta)])$. However, the adversarial loss in Eqn. (8) ensures that given a well-learned encryption module g, it is challenging to learn a powerful discriminator D' to distinguish the real features from others.

Strategy 2: The adversary tries to directly decode the targeted input from the encrypted feature that $\hat{I} = \text{dec}(x)$. Then we prove that the adversarial-learning loss in Eqn. (8) also boosts the difficulty of learning a powerful decoder $\hat{I} = \text{dec}(x)$. Let $g = g^*$ and $D = D^*$ denote the optimized encryption module and the discriminator according to Eqn. (8). Based on the encryption module g, we can construct a discriminator as $\hat{D}(a') = -\|g^*(I) - g^*(\text{dec}(a'))\|$. Because D^* is learned via $D^* = \arg\max_D L(g^*, \{b_I\}, D)$, we get $L(g^*, \{b_I\}, D^*) \geq L(g^*, \{b_I\}, \hat{D})$. The adversarial loss in Eqn. (8) provides the upper bound of $L(g^*, \{b_I\}, \hat{D})$, and thus restricts the capability of the decoder.

4. Experiments

In experiments, we applied our privacy-preserving approach to eight CNNs with classical structures to demonstrate the broad applicability of the proposed method. Without loss of generality, we tested on tasks such as object classification and face attribute estimation, and the method can also be

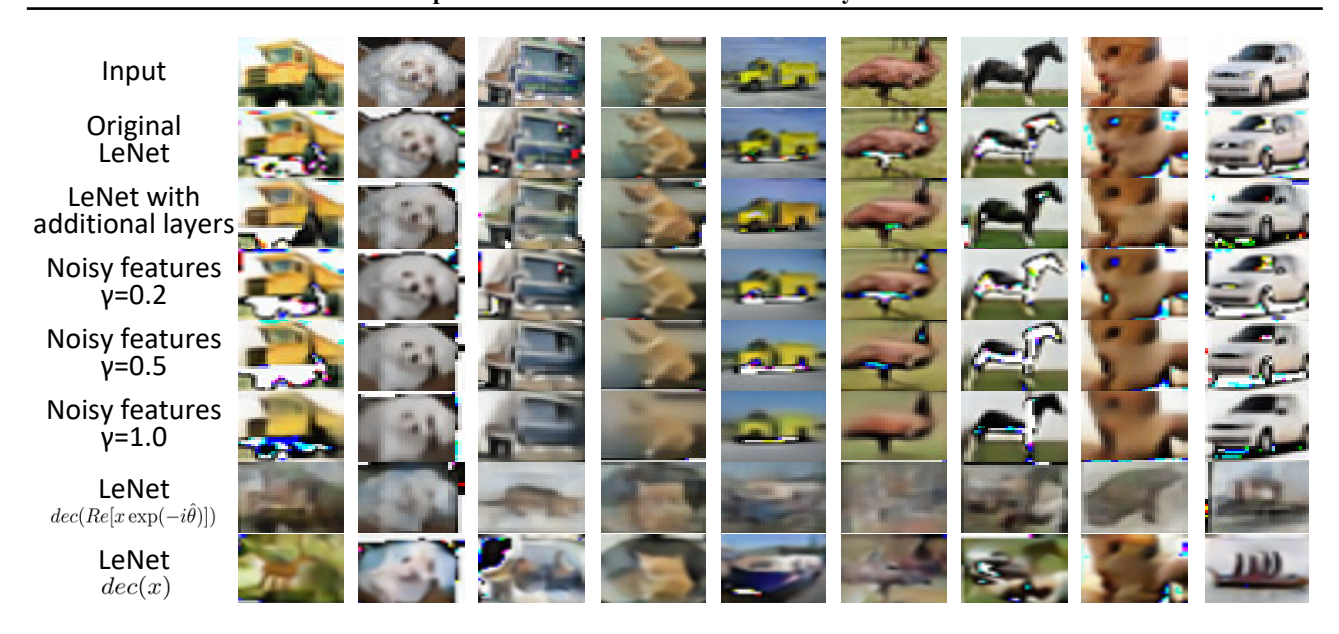


Figure 3. CIFAR-10 images reconstructed from 'encrypted' features on a variety of LeNet-based neural networks.

		Classification Error Rates			Reconstruction Errors				
	Dataset	Original	Network with	Ours	Original	Network with	Ours	Ours	
		network	additional layers		network	additional layers	$\operatorname{dec}(\Re[x\exp(-i\hat{\theta})])$	dec(x)	
ResNet-20- α	CIFAR-10	11.56	9.68	10.91	0.0906	0.1225	0.2664	0.2420	
ResNet-20- β	CIFAR-10	11.99	9.79	12.28	0.0967	0.1210	0.2424	0.2420	
ResNet-32- α	CIFAR-10	11.13	9.67	10.48	0.0930	0.1171	0.2569	0.2412	
ResNet-32- β	CIFAR-10	10.91	9.40	11.12	0.0959	0.1189	0.2515	0.2425	
ResNet-44- α	CIFAR-10	10.67	9.43	11.08	0.0933	0.1109	0.2746	0.2419	
ResNet-44- β	CIFAR-10	10.50	10.15	10.51	0.0973	0.1210	0.2511	0.2397	
ResNet-56- α	CIFAR-10	10.17	9.16	11.53	0.0989	0.1304	0.2804	0.2377	
ResNet-56- β	CIFAR-10	10.78	9.04	11.28	0.0907	0.1176	0.2585	0.2358	
ResNet-110- α	CIFAR-10	10.19	9.14	11.97	0.0896	0.1079	0.3081	0.2495	
ResNet-110- β	CIFAR-10	10.21	9.36	11.85	0.0932	0.1152	0.2582	0.2414	

Table 1. Experimental results based on residual networks using the CIFAR-10 dataset.

applied to deep models for other tasks.

We evaluate our approach from two aspects: the performance of the task and the privacy-preserving performance. The latter was measured by three metrics under two typical inversion strategies, as well as the qualitative visualization of the recovered inputs. We compared the proposed method with three baselines. Experimental results demonstrated the superior performance of our method in privacy protection to baselines with a very limited decrease of the discrimination power.

4.1. Implementation Details

We revised a neural network into a complex-valued neural network as follows. First, the neural network was divided into the encryption, processing, and decryption modules. The division of each network will be introduced later. Second, an adversarial learning module was attached to the first few layers composing the encryption module. The adversarial learning module included a generator and a discriminator. The generator consisted of a convolutional layer with $3\times 3\times K$ filters, and the discriminator was composed by a convolutional layer as well as a fully-connected layer. The output of the generator was rotated by a randomly selected angle before feeding to the processing module.

To adapt to complex-valued features, in the processing module of the residual networks, we set c=1 for the revised non-linear layers $\delta(\cdot)$. Except for the residual networks, other baseline neural networks did not contain normalization layers in the processing module, so we set $c_k = \mathbb{E}_{ij} \|x'_{ijk}\|$ for neural activations in the k-th channel.

Modular division of neural networks: In total, we revised eight neural networks: the 1st to the 5th are residual networks (He et al., 2016) with 20, 32, 44, 56, 110 convolutional layers, which are termed *ResNet-20*, *ResNet-32*,

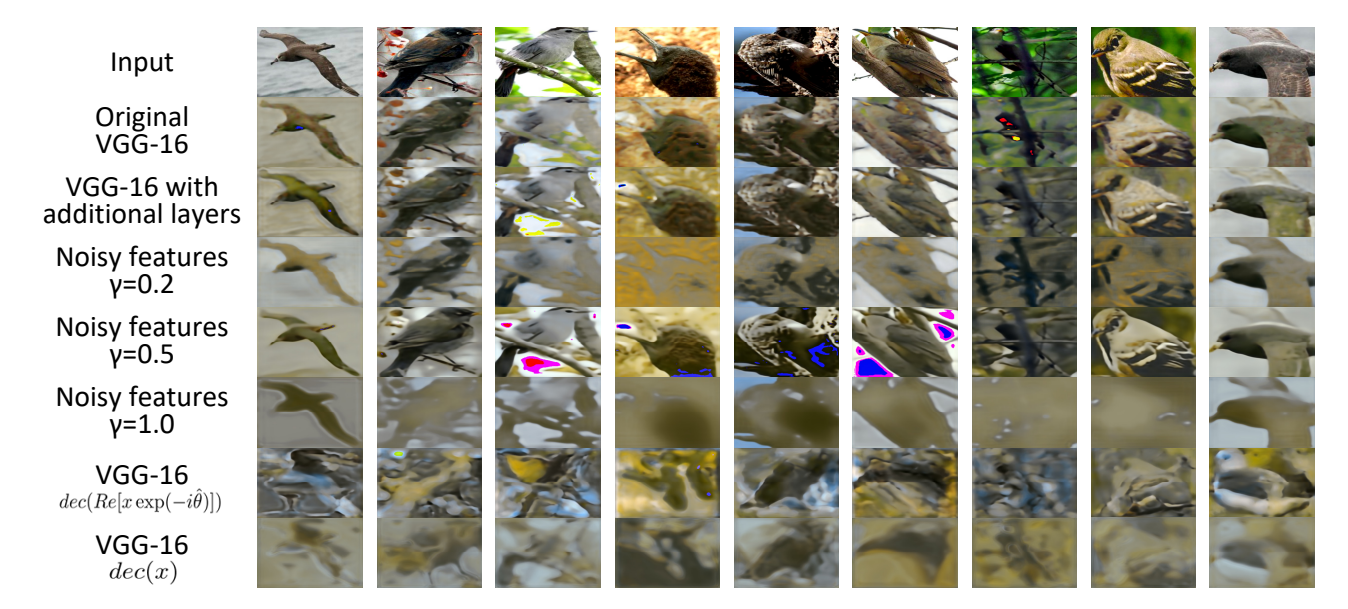


Figure 4. CUB200-2011 images reconstructed from 'encrypted' features on a variety of VGG-16-based neural networks.

ResNet-44, *ResNet-56*, and *ResNet-110*, respectively. The 6th, 7th, and 8th neural networks were the LeNet (LeCun et al., 1998), the VGG-16 (Simonyan & Zisserman, 2015), and the AlexNet (Krizhevsky et al., 2012), respectively.

The assignment of the encryption/processing/decryption modules of each network is as follows. For the residual network, we tested two variations of it — ResNet- α and ResNet- β . In the ResNet- α network, the output of the layer before the first 16×16 feature map was fed to the adversarial learning module, and thus its encryption module included the adversarial learning module and the layers before it. Layers following the first 8×8 feature map constituted the decryption module. All layers in between were the processing module. In the ResNet- β network, the encryption and processing modules were the same as the ResNet- α , while the last residual block with its following layers constituted the decryption module.

For the LeNet, the encryption module consisted of the first convolutional layer as well as the adversarial-learning module, while the decryption module contained the softmax layer. The VGG-16 used all layers before the last 56×56 feature map and the adversarial-learning module as its encryption module. Fully-connected layers and the softmax layer were the decryption module. For the AlexNet, the output of the first three conv-layer was fed into the adversarial learning module as the encryption module, and the decryption module included fully-connected layers and the softmax layer.

Decoder networks: Two decoder networks were implemented following two inversion-attack strategies in Section 3.2. Both of them were revised from U-net structures.

The original U-net (Ronneberger et al., 2015) consists of eight blocks, and we revised each block to contain six convolutional layers for better reconstruction performance.

4.2. Datasets

We applied our approach to object classification (or fine-grained classification) on three datasets, *i.e.* the CIFAR-10, CIFAR-100 (Krizhevsky, 2009) and CUB200-2011 (Wah et al., 2011) datasets. In addition, we also conducted face attribute estimation on the CelebA dataset (Liu et al., 2015).

The CIFAR-10 dataset consists of 60K 32×32 color images in 10 classes, with 6000 images per class. There are 50K training images and 10K test images in the dataset. The CIFAR-100 dataset has 100 classes containing 500 training and 100 testing images per class. The CUB200-2011 dataset contains a total of 11.8K bird images of 200 species for finegrained classification. All bird images in the CUB200-2011 datasets were cropped using their bounding boxes for both training and testing. Implementation-wise, the final layer of the decryption module in each neural network was revised to output the correct number of categories, which are 10, 100, 200 respectively for the three datasets. The average top-1 classification accuracy was reported for evaluation.

The CelebA dataset contains more than 200K celebrity images, each with 40 attribute annotations. The dataset covers large pose variations and background clutter with great diversity, a large quantity and rich annotations. Face images in the CelebA dataset were all cropped using their bounding boxes for both training and testing. The final layer of the decryption module was revised to produce 40 attributes for each facial image. The average estimation error rate for

Input Original AlexNet AlexNet with additional layers $\begin{array}{c} \text{AlexNet } \\ \text{Alex}(Re[x\exp(-i\hat{\theta})]) \\ \text{AlexNet } \\ dec(x) \end{array}$

Figure 5. CelebA images reconstructed from 'encrypted' features on a variety of AlexNet-based neural networks.

Classification Error Rates									
	Dataset	Original	Network with	Noise feature	Noise feature	Noise feature	Ours		
		network	additional layers	$\gamma = 0.2$	$\gamma = 0.5$	$\gamma = 1.0$			
LeNet	CIFAR-10	19.78	21.52	24.15	27.53	34.43	17.95		
LeNet	CIFAR-100	51.45	49.85	56.65	67.66	78.82	49.76		
ResNet-56- α	CIFAR-100	53.26	44.38	57.24	61.31	74.17	44.37		
ResNet-110- α	CIFAR-100	50.64	44.93	55.19	61.12	71.31	50.94		
VGG-16	CUB-200	56.78	63.47	69.20	99.48	99.48	78.50		
AlexNet	CelebA	14.17	9.49	_	_	_	15.94		
Reconstruction Errors									
	Dataset	Original	Network with	Noise feature	Noise feature	Noise feature	Ours	Ours	
		network	additional layers	$\gamma = 0.2$	$\gamma = 0.5$	$\gamma = 1.0$	$\operatorname{dec}(\Re[x\exp(-i\hat{\theta})])$	dec(x)	
LeNet	CIFAR-10	0.0769	0.1208	0.0948	0.1076	0.1274	0.2405	0.2353	
LeNet	CIFAR-100	0.0708	0.1314	0.0950	0.1012	0.1286	0.2700	0.2483	
ResNet-56- α	CIFAR-100	0.0929	0.1029	0.1461	0.1691	0.2017	0.2593	0.2473	
ResNet-110- α	CIFAR-100	0.1050	0.1092	0.1483	0.1690	0.2116	0.2602	0.2419	
VGG-16	CUB-200	0.1285	0.1202	0.1764	0.0972	0.1990	0.2803	0.2100	
AlexNet	CelebA	0.0687	0.1068	_	_	_	0.3272	0.2597	

Table 2. Experimental results.

all attributes of all facial images was used to evaluate the performance of a neural network.

4.3. Baselines

We compared our proposed method against three baselines from both perspectives of the model utility and the privacy protection. These baseline neural networks were constructed on the basis of the neural network structures described in Section 4.1, but were tweaked for different purposes. Fig. 2 gives an overview of the baseline network structures. For a fair comparison, each group of neural networks in comparisons were divided in the same way.

The first baseline (the top one in Fig. 2) was the original neural network, from which our complex-valued network was modified. The neural network did not contain any

adversarial-learning module without modifying functions of its intermediate layers.

In the second baseline network, we injected noises to the features released by the "encryption" module. The quotes indicate that there was no actual encryption going on, but the noisy feature $a+\gamma\cdot\epsilon$ was fed to the next layer instead of a, serving as a perturbation-based privacy-preserving method. Here ϵ represented a high-dimensional random noise vector with the same average activation magnitude as a. We set $\gamma=0.5,1.0,2.0$ respectively, indicating the low, medium, and high levels of noises.

Owing to the adversarial-learning module, the complexvalued neural network consisted of additional layers which may affect the task performance. To enable a fair comparison, our third baseline network structure was constructed

	Dataset	Ours
ResNet-20- α	CIFAR-10	0.7890
ResNet-20- β	CIFAR-10	0.7859
ResNet-32- α	CIFAR-10	0.7820
ResNet-32- β	CIFAR-10	0.7843
ResNet-44- α	CIFAR-10	0.8411
ResNet-44- β	CIFAR-10	0.7853
ResNet-56- α	CIFAR-10	0.8088
ResNet-56- β	CIFAR-10	0.8283
ResNet-110- α	CIFAR-10	0.8048
ResNet-110- β	CIFAR-10	0.7818
LeNet	CIFAR-10	0.7884
LeNet	CIFAR-100	0.8046
ResNet-56- α	CIFAR-100	0.7898
ResNet-110- α	CIFAR-100	0.7878
VGG-16	CUB-200	1.5572
AlexNet	CelebA	0.8500

Table 3. Average error of the estimated rotation angle θ .

by adding layers, which were the same as the adversarial-learning module but did not contain the adversarial-learning loss.

To test the privacy-protection performance, we mimicked an adversary trying to reconstruct the input from features released by the encryption module. In the experiments, we respectively trained decoder networks for each group of neural networks shown in Fig. 2. The decoder network followed the structure as described in Section 4.1, but took the input-feature pairs as inputs. For the complex-valued neural network, we applied the two decoding strategies $\operatorname{dec}(\Re[x\exp(-i\hat{\theta})])$ and $\operatorname{dec}(x)$, as introduced in Section 3.2 to reconstruct the input.

Adversary decoders can be learned as follows. An adversary can prepare a set of training samples, and repeatedly send each training sample I several times to our encryption module to retrieve the corresponding encrypted features for I. Theoretically, the true phase θ^* and the original feature a can be recovered. Given I, a, and θ^* , a decoder can be learned to invert features.

4.4. Experimental Results

Our experimental results are summarized in Tables 1, 2, 3, 4, and results of feature inversion are visualized in Figs. 3, 4, 5. The results show that our method outperformed all baselines in privacy performance, at the cost of a limited decrease of the task accuracy.

Three metrics were used to evaluate the privacy performance of a neural network. The first metric was the pixel-level reconstruction error $\mathbb{E}_{ijk}|\hat{I}_{ijk}-I_{ijk}|$, where I was the ground-truth, and \hat{I} denoted the reconstructed input: values of the in-

put were normalized to the range of $0 \le I_{ijk} \le 1$. The second metric was given as the expected value of $|\theta^* - \hat{\theta}|$, where $\hat{\theta} = \max_{\theta} D'(\Re[x \exp(-i\theta)])$, indicating the difficulty of recovering the true phase from the encrypted feature. The third metric was the failure rate of image re-identification — we asked five human annotators to view mixed pairs of the original inputs and the reconstructed inputs to decide whether or not they could use the reconstruction result to identify the input. The average failure rate of image re-identification was reported over all annotators.

Tables 1 and 2 list classification errors and reconstruction errors w.r.t. different neural network structures across datasets. Table 3 reports the error of the estimated best rotation angle. Table 4 shows the failure rate of image re-identification based on reconstructed images, which were labeled by human annotators. All these results demonstrate that our method exhibited significant superior performance in privacy protection to baselines. Compared to baseline networks with noisy features, our complex-valued features better preserved the discrimination power of the original neural network while better preventing the adversary from recovering the input.

5. Conclusion and Discussions

In this paper, we focus on the privacy-preserving problem of intermediate-layer neural network features being transferred from local devices to public clouds. We develop a novel method which transforms a traditional neural network into a complex-valued one, preventing the adversary from recovering input information from the processed features. Our method has been tested on a variety of datasets and neural networks, and shows superior performance in defending feature inversion attacks with only moderate loss of accuracy.

Theoretically, not only the encrypted feature, but also all other intermediate-layer features in the processing module can preserve privacy. However, we only need to invert the encrypted feature to test the privacy-preserving performance, since all features in following layers can be regarded as functions of the encrypted feature. Thus, we can roughly consider the encrypted feature's performance as the lower bound of other features.

Our method can be considered to conform to k-anonymity in the sense that the encrypted feature cannot be distinguished from at least k-1 other synthetic features.

References

Abadi, M., Chu, A., Goodfellow, I., McMahan, H. B., Mironov, I., Talwar, K., and Zhang, L. Deep Learning with Differential Privacy. In *Proc. of the 2016 ACM*

	Dataset	Original	w/ additional	$\gamma = 0.2$	$\gamma = 0.5$	$\gamma = 1.0$	Ours	Ours
		network	layers				$dec(Re[x\exp(-i\hat{\theta})])$	dec(x)
LeNet	Cifar-10	0.16	0.12	0.20	0.20	0.24	0.82	0.92
LeNet	CIFAr-100	0.16	0.14	0.20	0.64	0.72	0.80	0.92
ResNet-56- α	CIFAR-100	0.06	0.06	0.08	0.10	0.36	0.72	0.88
ResNet-110- α	CIFAR-100	0.04	0.12	0.10	0.16	0.36	0.80	0.86
VGG-16	CUB-200	0.06	0.06	0.08	0.02	0.14	0.86	0.84
AlexNet	CelebaA	0.04	0.24	_	_	_	0.96	1.00

Table 4. Failure rate of image re-identification.

- SIGSAC Conference on Computer and Communications Security (CCS), pp. 308–318. ACM, 2016.
- Arjovsky, M., Chintala, S., and Bottou, L. Wasserstein Generative Adversarial Networks. In *Proceedings of the 34th International Conference on Machine Learning*, pp. 214–223, 2017.
- Danihelka, I., Wayne, G., Uria, B., Kalchbrenner, N., and Graves, A. Associative Long Short-Term Memory. 2016.
- Dosovitskiy, A. and Brox, T. Inverting Visual Representations with Convolutional Networks. In *Proc. of the IEEE Conference on Computer Vision and Pattern Recognition (CVPR)*, pp. 4829–4837, 2016.
- He, K., Zhang, X., Ren, S., and Sun, J. Deep residual learning for image recognition. *In CVPR*, 2016.
- Krizhevsky, A. Learning multiple layers of features from tiny images. Technical report, 2009.
- Krizhevsky, A., Sutskever, I., and Hinton, G. E. Imagenet classification with deep convolutional neural networks. In *Advances in Neural Information Processing Systems* (*NIPS*), pp. 1097–1105, 2012.
- LeCun, Y., Bottou, L., Bengio, Y., and Haffner., P. Gradient-based learning applied to document recognition. *In Proceedings of the IEEE*, 1998.
- Li, M., Lai, L., Suda, N., Chandra, V., and Pan, D. Z. PrivyNet: A Flexible Framework for Privacy-Preserving Deep Neural Network Training. arXiv preprint arXiv:1709.06161, 2017.
- Liu, Z., Luo, P., Wang, X., and Tang, X. Deep learning face attributes in the wild. *In ICCV*, 2015.
- Mahendran, A. and Vedaldi, A. Understanding deep image representations by inverting them. *In CVPR*, 2015.
- Mohassel, P. and Zhang, Y. SecureML: A System for Scalable Privacy-Preserving Machine Learning. In 2017 38th IEEE Symposium on Security and Privacy (SP), pp. 19–38. IEEE, 2017.

- Osia, S. A., Shamsabadi, A. S., Taheri, A., Katevas, K., Sajadmanesh, S., Rabiee, H. R., Lane, N. D., and Haddadi, H. A Hybrid Deep Learning Architecture for Privacy-Preserving Mobile Analytics. *arXiv preprint arXiv:1703.02952*, 2017.
- Reichert, D. P. and Serre, T. Neuronal Synchrony in Complex-Valued Deep Networks. *arXiv preprint arXiv:1312.6115*, 2013.
- Ronneberger, O., Fischer, P., and Brox, T. U-net: Convolutional networks for biomedical image segmentation. *In CVPR*, 2015.
- Shokri, R. and Shmatikov, V. Privacy-preserving Deep Learning. In *Proc. of the 22nd ACM SIGSAC Conference* on Computer and Communications Security (CCS), pp. 1310–1321. ACM, 2015.
- Simonyan, K. and Zisserman, A. Very deep convolutional networks for large-scale image recognition. *In ICLR*, 2015.
- Simonyan, K., Vedaldi, A., and Zisserman, A. Deep inside convolutional networks: visualising image classification models and saliency maps. *In arXiv:1312.6034*, 2013.
- Song, S., Chaudhuri, K., and Sarwate, A. D. Stochastic Gradient Descent with Differentially Private Updates. In *Proc. of the 2013 IEEE Global Conference on Signal and Information Processing (GlobalSIP)*, pp. 245–248. IEEE, 2013.
- Trabelsi, C., Bilaniuk, O., Zhang, Y., Serdyuk, D., Subramanian, S., Santos, J. F., Mehri, S., Rostamzadeh, N., Bengio, Y., and Pal, C. J. Deep Complex Networks. 2018.
- Wah, C., Branson, S., Welinder, P., Perona, P., and Belongie, S. The caltech-ucsd birds-200-2011 dataset. Technical report, In California Institute of Technology, 2011.
- Wang, J., Zhang, J., Bao, W., Zhu, X., Cao, B., and Yu, P. S. Not Just Privacy: Improving Performance of Private Deep Learning in Mobile Cloud. In *Proc. of the 24th ACM SIGKDD International Conference on Knowledge Discovery & Data Mining*, pp. 2407–2416. ACM, 2018.

- Zeiler, M. D. and Fergus, R. Visualizing and understanding convolutional networks. *In ECCV*, 2014.
- Zhang, Q., Yang, L. T., and Chen, Z. Privacy preserving deep computation model on cloud for big data feature learning. *IEEE Transactions on Computers*, 65(5):1351–1362, 2016.

Proof of
$$\Phi(e^{i\theta}x) = e^{i\theta}\Phi(x)$$

In this paper, we design the processing module to ensure features of all layers are rotated by the same angle, in order to enable the later decryption of the feature.

$$\begin{cases} x^{(0)} = a + bi \\ x^{(\theta)} = e^{i\theta} x^{(0)} \end{cases} \Rightarrow \forall j, \ f_j^{(\theta)} = e^{i\theta} f_j^{(0)}$$

where $f_j^{(\theta)}$ and $f_j^{(0)}$ represent the feature map computed using the input $x^{(\theta)}$ and that computed using the input $x^{(0)}$, respectively.

In order to prove the above equation, we revise basic layers/operations in the processing module to ensure

$$\Phi(e^{i\theta}x) = e^{i\theta}\Phi(x)$$

where $\Phi(\cdot)$ denotes the function of a certain layer/operation. x is given as the input of the specific layer/operation $\Phi(\cdot)$. Based on this equation, we can recursively prove $f_i^{(\theta)} = e^{i\theta} f_i^{(0)}$.

Let us consider the following six commonest types of layers/functions to construct the processing module, *i.e.* the conv-layer, the ReLU layer, the batch-normalization layer, the average/max pooling layer, the dropout layer, and the skip-connection operation.

1. We revise the conv-layer by omitting the bias term. Thus, we get

$$\Phi(e^{i\theta}x) = w \otimes [e^{i\theta}x] = e^{i\theta}[w \otimes x] = e^{i\theta}\Phi(x)$$

2. We replace the ReLU layer with the non-linear activation function of $\phi(x_{ijk}) = \frac{\|x_{ijk}\|}{\max\{\|x_{ijk}\|,c\}} \cdot x_{ijk}$. Thus, we can write the element-wise operation as follows.

$$\phi(e^{i\theta}x_{ijk}) = \frac{\|e^{i\theta}x_{ijk}\|}{\max\{\|e^{i\theta}x_{ijk}\|, c\}} \cdot [e^{i\theta}x_{ijk}] = e^{i\theta} \left[\frac{\|x_{ijk}\|}{\max\{\|x_{ijk}\|, c\}} \cdot x_{ijk} \right] = e^{i\theta} \phi(x_{ijk})$$

3. We replace the batch-normalization layer with the function of $\phi(x_{ijk}^l) = \frac{x_{ijk}^l}{\sqrt{\mathbb{E}_{ijl}[\|x_{ijk}^l\|^2]}}$. Thus, we can write the element-wise operation as follows.

$$\phi(e^{i\theta}x_{ijk}^{l}) = \frac{e^{i\theta}x_{ijk}^{l}}{\sqrt{\mathbb{E}_{ijl}[\|e^{i\theta}x_{ijk}^{l}\|^{2}]}} = e^{i\theta}\left[\frac{x_{ijk}^{l}}{\sqrt{\mathbb{E}_{ijl}[\|x_{ijk}^{l}\|^{2}]}}\right] = e^{i\theta}\phi(x_{ijk}^{l})$$

4. For the average/max pooling layer and the dropout layer, we can represent their functions in the form of $\Phi(x) = Ax$, where x is given as a vectorized feature, and A denotes a matrix. For the average/max-pooling operation, A represents the selection of neural activations. For the dropout layer, A contains binary values that indicate the dropout state. In this way, we get

$$\Phi(e^{i\theta}x) = A(e^{i\theta}x) = e^{i\theta}[Ax] = e^{i\theta}\Phi(x)$$

5. For the skip-connection operation, we get

$$\Phi(e^{i\theta}x) = e^{i\theta}x + \Psi(e^{i\theta}x) = e^{i\theta}[x + \Psi(x)] = e^{i\theta}\Phi(x)$$

where $\Psi(\cdot)$ denotes the function that is skipped by the connection. We can recursively ensure $\Psi(e^{i\theta}x) = e^{i\theta}\Psi(x)$.